Full Bagasse Bio-Waste Derived 3D Photothermal Aerogels for High Efficient Solar Steam Generation

Jun Xiong
College of Chemistry and Chemical Engineering, Wuhan Textile University
Zhenning Zhang
Wuhan Textile University
Yuhao Liu
Wuhan Textile University
Jie Yi
Wuhan Textile University
Yixin Wang
Wuhan Textile University
Bowen Li
Wuhan Textile University
Weiming Wang
Wuhan Textile University
Shuai Peng
Wuhan Textile University
Xue Min
Wuhan Textile University
Yunyun Gui
Wuhan Textile University
Ming Li (lim@wtu.edu.cn)
Wuhan Textile University https://orcid.org/0000-0003-2476-7727
Junjun Peng
Wuhan Textile University

Research Article

Keywords: Solar steam generation, Bio-waste, Photothermal materials, Bagasse, Aerogels

Posted Date: July 6th, 2021

DOI: https://doi.org/10.21203/rs.3.rs-653183/v1

Version of Record: A version of this preprint was published at Cellulose on November 25th, 2021. See the published version at https://doi.org/10.1007/s10570-021-04323-6.

Abstract

Nowadays, freshwater shortage, energy crisis and environmental pollution are the three major threats to human beings. Herein, we develop a photothermal material based on bagasse for solar steam generation to relieve freshwater crisis and mitigate environmental pollution caused by bio-waste. The mainly functional part of the solar driven steam generator in this paper is bagasse-based photothermal aerogel (B-PTA), which composes of carbonized bagasse (CB) and bagasse-derived cellulose fiber (BDCF). The B-PTA with CB can effectively absorb solar (~95%) and has an excellent light-to-heat ability. The B-PTA with DBCF has super-hydrophilicity, water transport and retention ability. Depending on the excellent light absorption and 3D water passageway, the B-PTA gives a water evaporation rate of 1.36 kg m^{-2} h^{-1}, and can achieve a photothermal conversion efficiency of 77.34% under 1-sun illumination (1 kW m^{-2}). The B-PTA has excellent stability that the efficiency without significant decrease after 20 cycles. In addition, the B-PTA can effectively desalt seawater and purify dye wastewater with natural sunlight. Therefore, turning bio-waste into valuable photothermal material for solar steam generation is possible. Due to the merits of low cost, scalability, environmental friendliness, B-PTA has the potential for real-world water purification.

Introduction

The freshwater shortage, energy crisis, environmental pollution are the three main challenges facing human beings in modern society (Delgado et al. 2020; Lewis 2007; Mir and Bicer 2021). In spite of the fact, nearly three-quarters of the world is covered by water, the vast majority of the Earth's water is mostly in the oceans and is saline, resulting in less than 1% of water can be directly available by residents, and more than one-third of the world's population is affected by freshwater scarcity (Liu et al. 2018; Ma et al. 2020; Ridoutt and Pfister 2010). Therefore, obtaining clean and hygienic water from seawater or wastewater is an urgent issue. Traditionally utilized water purification strategies, such as reverse osmosis membranes and thermal distillation technologies, require high cost and consume large amounts of energy (Feria-Díaz et al. 2021a; Feria-Díaz et al. 2021b). Solar energy, as a green and renewable resource, is inexhaustible and freely available on earth. Recently, interfacial solar steam generation (ISSG) as a promising desalination strategy has received extreme attention to moderate the global scarcity of freshwater. The key component of ISSG device is the interfacial photothermal materials (PTMs). Usually, the PTMs include three essential functions: (1) broadband light absorption capability with high light-to-heat conversion efficiency; (2) hydrophilic porous structure for rapid water transportation to the evaporating surface; (3) excellent chemical and thermal stability to satisfy the demand of the long-term applications. Various efforts have been devoted to investigating efficient PTMs for water purification. The PTMs that have been reported involved in ISSG can be classified into several categories: metallic plasmonic materials (Bae et al. 2015; Kiriarachchi et al. 2018; Liu et al. 2015; Zhou et al. 2016), semiconductor materials (Aziznezhad et al. 2020; Jiang et al. 2020; Wu et al. 2019; Zuo et al. 2021), and carbon-based materials (Li et al. 2017; Wang et al. 2020; Yang et al. 2020; Yin et al. 2021; Zhu et al. 2017). Due to the high cost of raw nanomaterials, instability in corrosive media, or complex preparation processes, the above-mentioned PTMs were restricted for widespread applications. Therefore, to achieve

practical applications, there is a high demand for the preparation of PTMs with simple methods, low cost, environmental friendliness and reusability. Bio-waste, with its freely available, abundant carbon and cellulose sources, which can be acted as light absorber and water transporter, respectively, is a good candidate and offers a potential solution for the development of PTMs for real-life applications.

Biomass is planted all over the world. According to statistics, the global annual production of biomass is about 146 billion tons, and a large amount of biomass byproducts are generated in agriculture and industry, such as the paper industry and forest mining (Alvarenga et al. 2019; Anderson et al. 2013; Börjesson et al. 2017). About 30 billion tons of bio-waste are yielded from agricultural production every year, which will cause serious environmental problems (Demirbaş 2005; Laurijssen et al. 2010). In contrast, bio-waste is an important energy resource for the preparation of coke and biochar (Abbasi and Abbasi 2010; Kang et al. 2019). Therefore, the rational exploitation of bio-waste can not only reduce environmental pollution but also alleviate the energy crisis. Recently, bio-waste has attracted great interest in the development of valuable PTMs due to its free availability, low toxicity, and abundant carbon and cellulose sources. Zhang reported carbonized lotus seedpods as solar steam generation without any thermally insulating layer, which exhibited excellent light absorption capacity that is close to 99%, and photothermal conversion efficiency can reach 86.5% under 1-sun irradiation (Fang et al. 2018). He also presented that the 3D-structured carbonized sunflower head has a high evaporation efficiency of 100.4%, and the evaporation rate can reach up to 1.51 kg m^{-2} h^{-1} under 1-sun (Sun et al. 2020). However, the poor mechanical property of carbonized bio-waste such as lotus seedpod and sunflower head is unsuitable for portable. Xu fabricated PTA composed of reduced graphene oxide, sodium alginate and cellulose fibers derived from bio-waste rice straw, effectively reduced the radiation energy loss and captured the environmental energy, and achieved a high evaporation rate of 2.25 kg m^{-2} h^{-1} with an energy conversion efficiency of 88.9% under 1-sun (Storer et al. 2020). More importantly, the PTA has the potential application in real life due to the merits of lightweight, portable, scalable and environmentally friendly. However, the obvious drawback is the expensive reduced graphene oxide. Liu exploited bio-waste rice straw as the carbon source to reduce cost and manufactured a solar steam generation device that mixed the bacterial cellulose and carbonized leaves of rice straw as the light absorber and designed the culms as excellent water pumps. The photothermal conversion efficiency can be up to 75.8% (Fang et al. 2019).

Bagasse, as a bio-waste, is the byproduct of the sugarcane processing industry, and is composed of approximately 50% cellulose, 25% hemicellulose and 25% lignin (Cardona et al. 2010; Sun 2004; Torgbo et al. 2021). Bagasse, as the source of carbon and cellulose, has the potential to be manufactured into photothermal aerogel (PTA). In this work, we exploited bagasse bio-waste to fabricate PTA, which is consisted of carbonized bagasse (CB) for light absorption and aerogel from bagasse fiber for water transportation (Fig. 1). This work investigated the relationship between the content of CB and photothermal conversion efficiency of bagasse-based photothermal aerogel (B-PTA), discovered that the B-PTA consists of 1g CB and 2 g bagasse fiber can achieve the optimal results that the water evaporation rates is 1.36 kg m^{-2} h^{-1} and the photothermal conversion efficiency is approximate 77.34% under 1-sun

illumination. The efficiency without significant decrease after 20 cycles. Furthermore, the solar steam generator can effectively desalt seawater and purify dye wastewater under natural sunlight. This strategy of using bagasse as the raw materials to fabricate B-PTA provides an idea of converting bio-waste into valuable materials, and alleviating the environmental pollution. In addition, the freely available bio-waste will facilitate the applications of the solar steam generator in the real world.

2. Experimental Section

2.1 Materials

Bagasse used in the experiments was obtained from a local sugarcane juicy store. Sodium alginate (SA) was purchased from Shanghai Aladdin Co., Ltd., China. Sodium hydroxide, sodium chloride, calcium chloride, potassium chloride, magnesium chloride, magnesium sulfate, methylene blue, hydrochloric acid and ethanol (> 95%) were supplied by Sinopharm Chemical Reagent Co., Ltd., China.

2.2 Preparation

2.2.1 Pretreatment of bagasse

Bagasse was rinsed with tap water and then soaked in ethanol for two days to remove the residual sucrose, and then the bagasse was washed with deionized water and dried at 80°C for one day.

2.2.2 Preparation of BC

Pretreated bagasse (5 g) was placed in a tube furnace for 2 hours at 600°C in N_2 atmosphere (about 30 ml min^{-1}) with a ramp rate of 5°C min^{-1}. The carbonized bagasse was soaked in 1 M HCl (30 mL) for 1 hour, and washed with deionized water to neutral. The treated bagasse was dried at 80°C for 2 hours, and put into the ball mill for 30 minutes to obtain the BC.

2.2.3 Preparation of BDCF

Pretreated bagasse (2 g) and 3 M sodium hydroxide solution (80 mL) were added to a 100 mL Teflon stainless steel autoclave. Following the autoclave was sealed and heated at 180°C for 12 hours. BDCF was obtained by filtering the resulting mixture and washing with deionized water to neutral.

2.2.4 Preparation of B-PTA

BDCF (2 g), BC (1 g) and 5 mg mL^{-1} SA (200 mL) were added to a 400 mL beaker and stirred for 20 minutes to obtain a mixture, which was added to a plastic container (height: 5 cm, diameter: 3 cm) for freeze-dried. The obtained samples were soaked in $CaCl_2$ solution (50 g L^{-1}) for 12 hours, washed several times with tap water and deionized, respectively, and then freeze-dried. Following the Ca^{2+} cross-linked aerogel was prepared named B-PTA-1 for solar steam generation. B-PTA-0, B-PTA-0.5 and B-PTA-1.5 were prepared with the above method by using 0 g, 0.5 g and 1.5 g BC, respectively.

2.3 Sample characterization

The morphology and structure of B-PTA were characterized using JEOL InTouchScope (JSM-IT500) scanning electron microscopy (SEM). XRD patterns were measured on a Rigaku Ultima IV diffractometer with a Cu Kα radiation source. Raman spectra characterization were carried out on a Themor DXR532 780 nm semiconductor laser. Fourier transform-infrared (FT-IR) spectra were measured by a Thermos Nicolet FT-IR spectrophotometer (model 6700). X-ray photoelectron spectroscopy (XPS) analysis was carried out on a Thermo Scientific K-Alpha^{+} with an aluminum potassium microaggregation monochromatic X-ray source. Static contact angles (SCAs) were measured by a contact angle meter (OAC20, DaraPhysics) through the static sessile drop method. UV-vis-NIR spectra were recorded by Solid Spec-3700 Shimadzu. The concentrations of Na^{+}, Mg^{2+}, K^{+} and Ca^{2+} were detected by inductively coupled plasma-optical emission spectroscopy (ICP-OES) using Agilent 730. UV-vis absorption spectra were carried out on TU-1950 Persee.

2.4 Solar steam generation experiments

Solar steam generation experiments were carried out at an ambient temperature of ~ 25°C and humidity of ~ 50% under laboratory conditions. B-PTA (height: 1 cm, diameter: 3 cm, Fig. S1) was placed on an EPE foam layer (EPE, height: 3 cm, diameter 5 cm) with a diameter 1.5 cm hole, which was filled with cotton cores for water transport. EPE foam was placed on a glass container (height: 7cm, diameter 5.2 cm) filled with tap water. The glass container was wrapped by EPE foam to prevent heat loss. Solar steam generation was performed with the help of a solar simulator (Perfect light, CHF500), and the mass change of tap water was recorded in real-time by an electronic balance (RADWAG, 0.0001 g in accuracy). Schematic illustration of detection water mass change was shown in Fig. S2. All the water purification experiments were carried out for 1 hour under constant 1-sun illumination. The temperature of the B-PTA was tracked using an infrared (IR) camera (Fluke, TiS60+). Simulated seawater was prepared as follows: 13.37 g of NaCl, 0.36 g of KCl, 1.13 g of $MgCl_2$, 0.58 g of $CaCl_2$ and 1.63 g of $MgSO_4$ were added to 500 mL deionized water and completely dissolved to obtain seawater for the desalination experiment. Methylene blue solution (20 mg L^{-1}) was prepared for the simulating experiments of purifying dye wastewater.

3. Results And Discussion

SEM images of the B-PTA-1 was measured, and 3D porous structure can be clearly observed as shown in Fig. 2a and 2b. The B-PTA-1 was composed of BC and BDCF as shown in Fig. 2c, and BC was disordered distribution on BDCF, which was entangled randomly to form an interconnected 3D porous structure. Compared with the B-PTA-1, the surface of BDCF in B-PTA-0 is smooth as shown in Fig. S3. The element mapping and energy dispersive X-ray (EDX) spectrum of the B-PTA-1 represented the major elements of C (73.79%), O(22.97%) and Ca (3.24 %) as shown in Fig. 2d and Fig S4. The XRD patterns of B-PTA-0, B-PTA-1 and BC were presented in Fig. 2e. In the diagram of B-PTA-0, 2-theta degrees were located at 16° and 22° corresponding to the (1 1 0) and (2 0 0) diffraction planes of cellulose, respectively (Mohiuddin et al. 2015; Rodriguez-Restrepo et al. 2020). The broad peak at 22.8° and weak peak at 44° of the BC were ascribed to (0 0 2) and (1 0 0) plane, respectively, suggested the formation of amorphous carbon (Sayed

et al. 2020). The characteristic diffraction peaks at 16°, 22.6° and 44.5° in the B-PTA-1 indicated the existence of cellulose and amorphous carbon. The XRD patterns of B-PTA-0.5 and B-PTA-1.5 were shown in Fig. S5. In the Raman spectra of B-PTA-1 (Fig. 2f), the peaks at 1340 cm^{-1} and 1580 cm^{-1} attributed to the disorder D-band of amorphous carbon and the in-plane sp^2 vibration of graphite crystal G-band, respectively (Zhu et al. 2019).

The surface chemical compositions and functional groups of the B-PTAs were researched through FT-IR and XPS. The FT-IR characteristic absorption peaks located at 3458, 2900, 1428, 1030 cm^{-1} can be assigned to the OH, CH_2, CH symmetrical deformation, and COC stretching vibration of cellulose, respectively as shown in Fig. 3a (Gao et al. 2020). A peak was observed at 1625 cm^{-1} that was related to C = O functional groups as a result of the natural aging of cellulose (Salama 2020). XPS analysis of B-PTA-1 was researched as shown in Fig. 3b and 3c. The major elements of the B-PTA-1 were carbon and oxygen. The high-resolution spectrum of the C 1s peak can be assigned into three components including aliphatic C-C, hydroxyl carbon C-O and carboxy carbon O-C = O, which were consistent with the FT-IR, and further indicated the hydrophilic property of the B-PTAs.

The hydrophilicity, water transport and storage capacity of B-PTAs are extremely important in the solar steam generation device. Hydrophilicity was further demonstrated through water contact angle measurement as shown in Fig. 3d. A water droplet was wetted immediately when was dropped onto the surface of B-PTA, which indicated that the B-PTAs were super-hydrophilicity. White B-PTA-0 was researched to clearly observe the water transport ability. Once the B-PTA-0 is touched with the water of the cotton core, the wetting process starts immediately. The B-PDA-0 was completely wetted within 30 seconds as shown in Fig. 3f, which demonstrated that the B-PTA-0 can effectively transport water in the interconnected hierarchical porous networks. Moreover, the water hold ability of B-PTA-1 was researched. 0.232 g B-PTA-1 (height: 1 cm, diameter: 3 cm) can hold a weight of approximately 5.305 g water, which was 23 times weight without any obvious deformation as shown in Fig. S6. The results manifested that the B-PTAs have super-hydrophilicity, water transport and capacity storage.

The light absorption abilities of B-PTAs were investigated through UV–Vis–NIR spectrophotometer and weighted by the standard air mass 1.5 global (AM 1.5 G) solar spectrum as shown in Fig. 4a. The average integrated absorption of B-PTA-0, B-PTA-0.5, B-PTA-1 and B-PTA-1.5 in the wavelength range from 300 to 2500 nm was 51%, 93%, 95% and 96%, respectively. In the whole spectrum, B-PTA-0.5 exhibited stronger light absorption than B-PTA-0, which indicated that the CB can effectively enhance the light absorption ability of the B-PTAs. In addition, the absorption ability of B-PTA-1 and B-PTA-1.5 was similar and slightly stronger than B-PTA-0.5, which implied that B-PTA-1 is the best candidate for solar steam generation. In consideration of the excellent light absorption abilities, the light to heat capacities of the B-PTAs were researched. The temperature change of the B-PTAs under 1-sun illumination was traced through IR camera. The top surface temperatures of B-PTA-0 increased from 29.1°C to 42.0°C in the first 1 minute, and kept up near 48.7°C continuing to light for 8 minutes as shown in Fig. 4b. Relatively, the top surface temperature of B-PTA-0.5, B-PTA-1 and B-PTA-1.5 sharply increased from 27.8°C, 28.8°C and 27.8°C to

62.4°C, 71.3°C and 71.3°C in the first 1 minute, respectively, and maintained near 81.2°C, 85.3°C and 84.9°C with the extension of illumination time to 8 minutes, which indicated that the light to heat ability was B-PTA-1.5 ≈ B-PTA-1 > B-PTA-0.5 > B-PTA-0. IR images of B-PTA-0 and B-PTA-1 was presented in Fig. 4c and 4d. When the light was off 1 minute, the top surface temperature of B-PTA-0 decreased to 33.6°C, and B-PTA-0.5, B-PTA-1, B-PTA-1.5 dropped sharply to 41.4°C, 39.1°C, 40.1°C, respectively. IR images of B-PTA-0.5 and B-PTA-1.5 were shown in Fig. S7. Furthermore, the rate of increase and decrease in temperature of B-PTA-1, B-PTA-1.5 was close and faster than B-PTA-0.5, which was further proved that the light to heat capacities was B-PTA-1.5 ≈ B-PTA-1 > B-PTA-0.5 > B-PTA-0. These results were consistent with the UV–Vis–NIR research.

Solar steam generation of the B-PTA-0, B-PTA-0.5, B-PTA-1 and B-PTA-1.5 were investigated and the top surface temperature of the wet B-PTAs was recorded by IR camera under 1-sun irradiation. The top surface temperature of the B-PTA-0 increased from 22.4°C to 27.8°C after 3 min irradiation, and continuously risen and kept at average 33.8°C after 15 min illumination as shown in Fig. 5a. An increase in the content of BC of the B-PTAs resulted in the top surface temperature rising under solar steam generation. Compared with the B-PTA-0, the top surface temperature of the B-PTA-0.5 was higher under the same time of illumination, and stabilized at average 37.0°C after 15 min irradiation. Similarly, the top surface temperature of the B-PTA-1 was higher than B-PTA-0.5, and kept at average 39.5°C after 15 min irradiation. For the B-PTA-1.5, the top surface temperature was similar to B-PTA-1, and stabilized around at 39.5°C after 15 min illumination even if the BC content was higher than B-PTA-1. These results were consistent with the UV–Vis–NIR and light to heat research, which implied that the B-PTA-1 has the optimal BC content for solar steam generation.

To systematically evaluate the photothermal ability, the evaporation rates and efficiencies of B-PTAs were accurately recorded through an electronic balance under 1-sun irradiation. The time-dependent water mass change plots of B-PTAs were presented in Fig. 5b. The mass change of water of B-PTA-0, B-PTA-0.5, B-PTA-1 and B-PTA-1.5 were 0.57 g, 0.85 g, 0.96 g and 0.96 g, respectively within 1 hour. The diameter of the B-PTAs is 3 cm. The calculated evaporation rates under 1-sun irradiation was 0.81, 1.20, 1.36 and 1.36 kg m^{-2} h^{-1}, respectively. The dark field evaporation rates of B-PTA-0, B-PTA-0.5, B-PTA-1 and B-PTA-1.5 was 0.25, 0.23, 0.24 and 0,24 kg m^{-2} h^{-1}, respectively. The solar energy conversion efficiency (η) was calculated through the following equations (Li et al. 2018a; Li et al. 2018b):

$$\eta = m(H_{LV} + Q)/I$$

$$H_{LV} = 1.91846 \times 10^6[T_1/(T_1\text{-}33.91)]^2$$

$$Q = c(T_1\text{-}T_0)$$

Where m stands for the net water evaporation rate (kg m^{-2} h^{-1}). H_{LV} represents the liquid-vapor phase change enthalpy. Q is the sensible heat (J kg^{-1}). I represents the power density of solar illumination. T_1 is the temperature of evaporation (K), T_0 is the initial temperature of the water. c is the specific heat

capacity of bulk water (4.2 J g^{-1} K^{-1}). The net evaporation rates of the B-PTA-0, B-PTA-0.5, B-PTA-1 and B-PTA-1.5 were calculated to be 0.56, 0.97, 1.12 and 1.12 kg m^{-2} h^{-1}, corresponding to energy conversion efficiencies of 38.38%, 66.81%, 77.34% and 77.47%, respectively as shown in Fig. 6a, demonstrated that the evaporation efficiency of the B-PTAs increase with the increase of BC content, and the B-PTA-1 is the best candidate for solar steam generation. The energy conversion efficiency of the B-PTA-1 is higher than the graphene and rice-straw-fiber-based 3D photothermal aerogel (high: 1 cm, diameter: 3 cm), which is 73.60% [31]. Therefore, using cheap bio-waste bagasse to replace expensive graphene to manufacture solar steam generation material is possible. In addition, the evaporation performance of the B-PTA-1 kept stable for 20 cycles with each cycle maintained for 1 hour as shown in Fig. 6b, and represented excellent stability for solar steam generation performance.

To prove the practical application of the B-PTA-1 in desalination, an apparatus for collecting evaporator water was designed to detect ion concentration of evaporation water under the natural sunlight. The diameter of B-PTA-1 in outdoor experiments is about 11 cm (Fig. S8), which can generate about 13 ml water under 1-sun irradiation for 1 hour in theory. During the water evaporation progress, the generated steam condensed into water drops and adhered to the surface of the spherical glass container as shown in Fig. S9, and about 80 mL evaporated water was collected from 9:00 to 18:00 on May 24th, 2021. The ion (Na^+, K^+, Ca^{2+}, Mg^{2+}) concentrations of evaporated water were tested through ICP-OES method as shown in Fig. 6c, which were significantly decreased to several orders of magnitude, which were satisfied the drinking water standard defined by WHO (Raymond-Whish et al. 2007). The desalinated water can be regarded as clean and safe. To evaluate the application of the B-PTA-1 in purification dye wastewater, methyl blue (20 mg/L) was employed as raw water for the evaporation testing. About 30 ml evaporated water was collected from 11:00 to 3:00 on May 25th, 2021 as shown in Fig. S10. The purified water becomes colorless, the characteristic absorption peaks of methyl blue are removed and the absorbance is close to zero, indicating extremely low concentration of the dyes as shown in Fig. 6d. The results manifested that the B-PTA-1 can effectively purify seawater wastewater and dye wastewater.

Conclusion

In summary, a solar steam generator was manufactured from bio-waste bagasse. CB was composited with bagasse fiber to form a porous structure, light absorbers and super-hydrophilicity aerogel. Photothermal efficiency of B-PTA was affected by the content of CB. B-PTA-1 had the optimal water evaporation rate, which was 1.36 kg m^{-2} h^{-1} with photothermal efficiency 77.34%. The B-PTA has excellent stability that the efficiency without significant decrease after 20 cycles. In addition, simulator seawater and dye wastewater can be effectively purified with the natural solar light. Collected desalination was satisfied the drinking water standards. Therefore, B-PTA has the potential applications in seawater desalinization and industrial wastewater treatment. Applying low cost, scalability, environmental friendliness B-PTA to practical application is possible. This work indicated that turning bagasse bio-waste into valuable solar steam generator for mitigating environmental pollution, energy short and freshwater crisis is promising.

Declarations

Acknowledgments This work was supported by the Nation Natural Science Foundation of China (51203125), Hubei Natural Science Foundation (2019CFC905) and the Science and Technology Research Project of the Department of Education of Hubei Province (D20191704).

Authors' contributions JX: Conceptualization, methodology, Writing–review & editing. ZZ: Characterization and analysis. YL: Synthesis and characterization. JY: Synthesis and characterization. YW: Synthesis and characterization. BL: SEM characterization. WW: Data analysis. SP: Methodology. XM: Conceptualization and methodology. YG. SEM analysis. ML: Conceptualization and supervision. JP: Data analysis and check the manuscript.

Supplementary material Supplementary data associated with this article can be found in the online version.

Conflict of interests The authors declare that they have no known competing financial interests or personal relationships that could have appeared to influence the work reported in this paper.

Informed consent This article does not contain any studies or researches with human participants nor animals performed by any of the authors which violate ethical standards.

References

1. Abbasi T, Abbasi SA (2010) Biomass energy and the environmental impacts associated with its production and utilization. Renew Sust Energ Rev 14(3):919–937
2. Alvarenga P, Rodrigues D, Mourinha C, Palma P, de Varennes A, Cruz N, Tarelho LAC, Rodrigues S (2019) Use of wastes from the pulp and paper industry for the remediation of soils degraded by mining activities: Chemical, biochemical and ecotoxicological effects. Sci Total Environ 686:1152–1163
3. Anderson N, Jones J, Page-Dumroese D, McCollum D, Baker S, Loeffler D, Chung W (2013) A comparison of producer gas, biochar, and activated carbon from two distributed scale thermochemical conversion systems used to process forest biomass. Energies 6(1):164–183
4. Aziznezhad M, Goharshadi E, Namayandeh-Jorabchi M (2020) Surfactant-mediated prepared VO2 (M) nanoparticles for efficient solar steam generation. Sol Energy Mater Sol Cells 211:110515
5. Bae K, Kang G, Cho SK, Park W, Kim K, Padilla WJ (2015) Flexible thin-film black gold membranes with ultrabroadband plasmonic nanofocusing for efficient solar vapour generation. Nat Commun 6:10103
6. Börjesson P, Hansson J, Berndes G (2017) Future demand for forest-based biomass for energy purposes in Sweden. For Ecol Manag 383:17–26
7. Cardona CA, Quintero JA, Paz IC (2010) Production of bioethanol from sugarcane bagasse: Status and perspectives. Bioresour Technol 101(13):4754–4766

8. Delgado M, López A, Cuartas M, Rico C, Lobo A (2020) A decision support tool for planning biowaste management systems. J Clean Prod 242:118460
9. Demirbaş A (2005) Influence of gas and detrimental metal emissions from biomass firing and co-firing on environmental impact. Energy Sources 27(15):1419–1428
10. Fang J, Liu J, Gu J, Liu Q, Zhang W, Su H, Zhang D (2018) Hierarchical porous carbonized lotus seedpods for highly efficient solar steam generation. Chem Mater 30(18):6217–6221
11. Fang Q, Li T, Chen Z, Lin H, Wang P, Liu F (2019) Full biomass-derived solar stills for robust and stable evaporation to collect clean water from various water-bearing media. ACS Appl Mater Interfaces 11(11):10672–10679
12. Feria-Díaz JJ, Correa-Mahecha F, López-Méndez MC, Rodríguez-Miranda JP, Barrera-Rojas J (2021a) Recent desalination technologies by hybridization and integration with reverse osmosis: A review. Water 13(10):1369
13. Feria-Díaz JJ, López-Méndez MC, Rodríguez-Miranda JP, Sandoval-Herazo LC, Correa-Mahecha F (2021b) Commercial thermal technologies for desalination of water from renewable energies: A state of the art review. Processes 9(2):262
14. Gao Y, Wang X, Li X, Dai H (2020) An antibacterial composite film based on cellulose acetate/TiO2 nanoparticles. New J Chem 44(47):20751–20758
15. Jiang H, Fang H, Wang D, Sun J (2020) Spray-coated commercial ptfe membrane from mos2/laf3/pdms ink as solar absorber for efficient solar steam generation. Solar RRL 4(6):2000126
16. Kang K, Qiu L, Sun G, Zhu M, Yang X, Yao Y, Sun R (2019) Codensification technology as a critical strategy for energy recovery from biomass and other resources - A review. Renew Sust Energ Rev 116:109414
17. Kiriarachchi HD, Awad FS, Hassan AA, Bobb JA, Lin A, El-Shall MS (2018) Plasmonic chemically modified cotton nanocomposite fibers for efficient solar water desalination and wastewater treatment. Nanoscale 10(39):18531–18539
18. Laurijssen J, Marsidi M, Westenbroek A, Worrell E, Faaij A (2010) Paper and biomass for energy? Resour Conserv Recycl 54(12):1208–1218
19. Lewis NS (2007) Toward cost-effective solar energy use. Science 315(5813):798–801
20. Li X, Li J, Lu J, Xu N, Chen C, Min X, Zhu B, Li H, Zhou L, Zhu S, Zhang T, Zhu J (2018a) Enhancement of Interfacial Solar Vapor Generation by Environmental Energy. Joule 2(7):1331–1338
21. Li X, Lin R, Ni G, Xu N, Hu X, Zhu B, Lv G, Li J, Zhu S, Zhu J (2018b) Three-dimensional artificial transpiration for efficient solar waste-water treatment. Nati Sci Rev 5(1):70–77
22. Li Y, Gao T, Yang Z, Chen C, Kuang Y, Song J, Jia C, Hitz EM, Yang B, Hu L (2017) Graphene oxide-based evaporator with one-dimensional water transport enabling high-efficiency solar desalination. Nano Energy 41:201–209
23. Liu W, Lim WH, Sun F, Mitchell D, Wang H, Chen D, Bethke I, Shiogama H, Fischer E (2018) Global freshwater availability below normal conditions and population impact under 1.5 and 2 ℃

stabilization scenarios. Geophys Res Lett 45(18):9803–9813

24. Liu Y, Yu S, Feng R, Bernard A, Liu Y, Zhang Y, Duan H, Shang W, Tao P, Song C, Deng T (2015) A bioinspired, reusable, paper-based system for high-performance large-scale evaporation. Adv Mater 27(17):2768–2774
25. Ma T, Sun S, Fu G, Hall JW, Ni Y, He L, Yi J, Zhao N, Du Y, Pei T, Cheng W, Song C, Fang C, Zhou C (2020) Pollution exacerbates China's water scarcity and its regional inequality. Nat Commun 11(1):650
26. Mir N, Bicer Y (2021) Integration of electrodialysis with renewable energy sources for sustainable freshwater production: A review. J Environ Manage 289:112496
27. Mohiuddin M, Sadasivuni KK, Mun S, Kim J (2015) Flexible cellulose acetate/graphene blueprints for vibrotactile actuator. RSC Advances 5(43):34432–34438
28. Raymond-Whish S, Mayer LP, O'Neal T, Martinez A, Sellers MA, Christian PJ, Marion SL, Begay C, Propper CR, Hoyer PB, Dyer CA (2007) Drinking water with uranium below the U.S. EPA water standard causes estrogen receptor-dependent responses in female mice. Environ Health Perspect 115(12):1711–1716
29. Ridoutt BG, Pfister S (2010) A revised approach to water footprinting to make transparent the impacts of consumption and production on global freshwater scarcity. Global Environ Change 20(1):113–120
30. Rodriguez-Restrepo YA, Rocha CMR, Teixeira JA, Orrego CE (2020) Valorization of passion fruit stalk by the preparation of cellulose nanofibers and immobilization of trypsin. Fiber Polym 21(12):2807–2816
31. Salama A (2020) Cellulose/silk fibroin assisted calcium phosphate growth: Novel biocomposite for dye adsorption. Int J Biol Macromol 165(Pt B):1970–1977
32. Sayed DM, El-Deab MS, Elshakre ME, Allam NK (2020) Nanocrystalline cellulose confined in amorphous carbon fibers as capacitor material for efficient energy storage. J Phys Chem C 124(13):7007–7015
33. Storer DP, Phelps JL, Wu X, Owens G, Khan NI, Xu H (2020) Graphene and rice-straw-fiber-based 3d photothermal aerogels for highly efficient solar evaporation. ACS Appl Mater Interfaces 12(13):15279–15287
34. Sun J (2004) Isolation and characterization of cellulose from sugarcane bagasse. Polym Degrad Stab 84(2):331–339
35. Sun P, Zhang W, Zada I, Zhang Y, Gu J, Liu Q, Su H, Pantelic D, Jelenkovic B, Zhang D (2020) 3d-structured carbonized sunflower heads for improved energy efficiency in solar steam generation. ACS Appl Mater Interfaces 12(2):2171–2179
36. Torgbo S, Quan VM, Sukyai P (2021) Cellulosic value-added products from sugarcane bagasse. Cellulose 28(9):5219–5240
37. Wang L, Wang H, Liu C, Xu Y, Ma S, Zhuang Y, Zhang Q, Yang H, Xu W (2020) Bioinspired cellulose membrane with hierarchically porous structure for highly efficient solar steam generation. Cellulose

27(14):8255–8267
38. Wu X, Robson ME, Phelps JL, Tan JS, Shao B, Owens G, Xu H (2019) A flexible photothermal cotton-CuS nanocage-agarose aerogel towards portable solar steam generation. Nano Energy 56:708–715
39. Yang T, Lin H, Lin K-T, Jia B (2020) Carbon-based absorbers for solar evaporation: Steam generation and beyond. Sustain Mater Techno 25:e00182
40. Yin M, Hsin Y, Guo X, Zhang R, Huang X, Zhang X (2021) Facile and low-cost ceramic fiber-based carbon-carbon composite for solar evaporation. Sci Total Environ 759:143546
41. Zhou L, Tan Y, Wang J, Xu W, Yuan Y, Cai W, Zhu S, Zhu J (2016) 3D self-assembly of aluminium nanoparticles for plasmon-enhanced solar desalination. Nat Photonics 10(6):393–398
42. Zhu M, Li Y, Chen G, Jiang F, Yang Z, Luo X, Wang Y, Lacey SD, Dai J, Wang C, Jia C, Wan J, Yao Y, Gong A, Yang B, Yu Z, Das S, Hu L (2017) Tree-inspired design for high-efficiency water extraction. Adv Mater 29(44):1704107
43. Zhu M, Yu J, Ma C, Zhang C, Wu D, Zhu H (2019) Carbonized daikon for high efficient solar steam generation. Sol Energy Mater Sol Cells 191:83–90
44. Zuo S, Xia D, Guan Z, Yang F, Cheng S, Xu H, Wan R, Li D, Liu M (2021) Dual-functional CuO/CN for highly efficient solar evaporation and water purification. Sep Purif Technol 254:117611

Figures

Figure 1

Schematic illustration depicting the fabrication of B-PTA for solar steam generation.

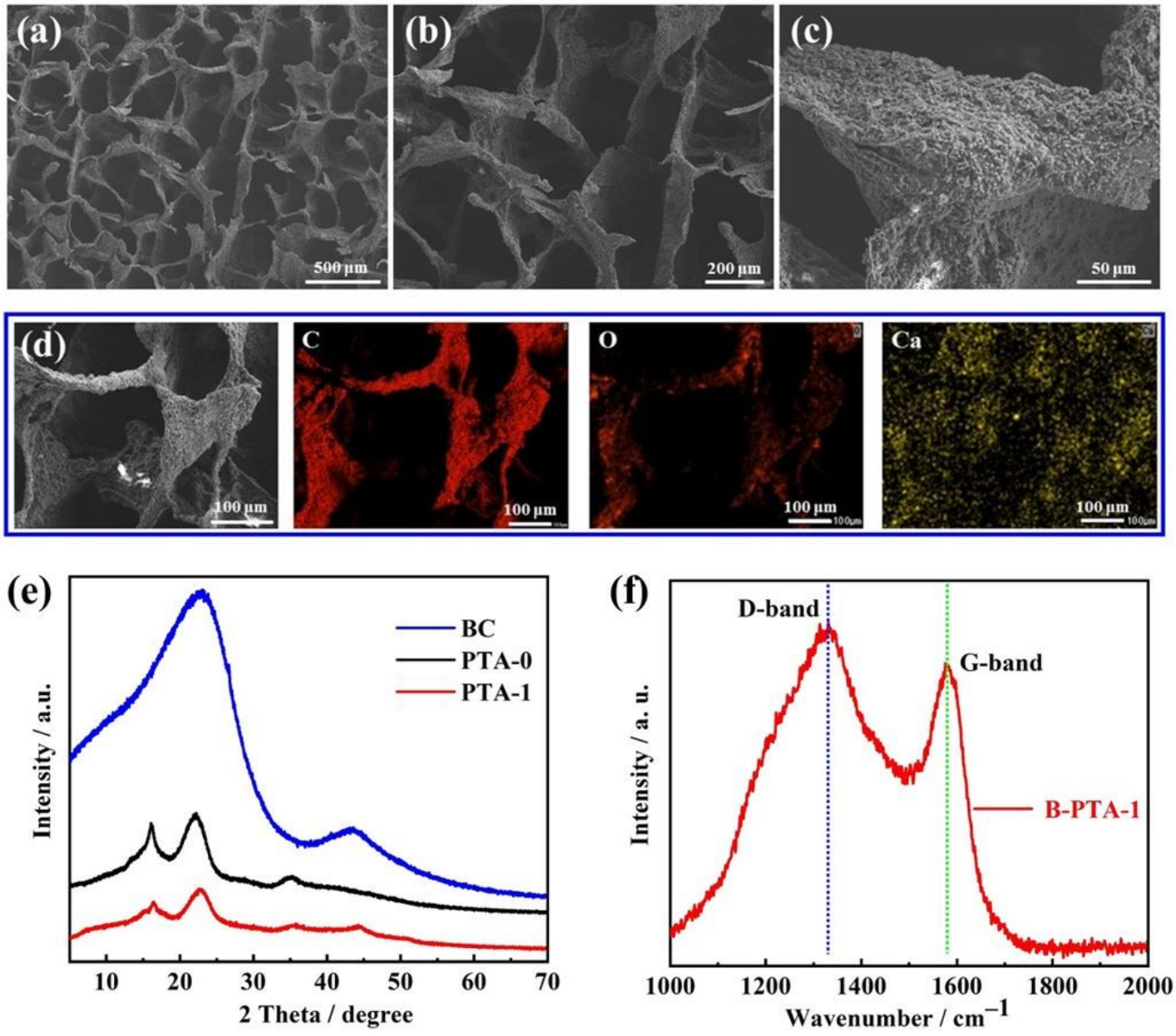

Figure 2

SEM images of B-PTA-1 at different magnifications (a-c); the element mapping of the B-PTA-1 (d); XRD patterns of B-PTA-0, B-PTA-1 and BC (e); Raman spectra of B-PTA-1 (f)

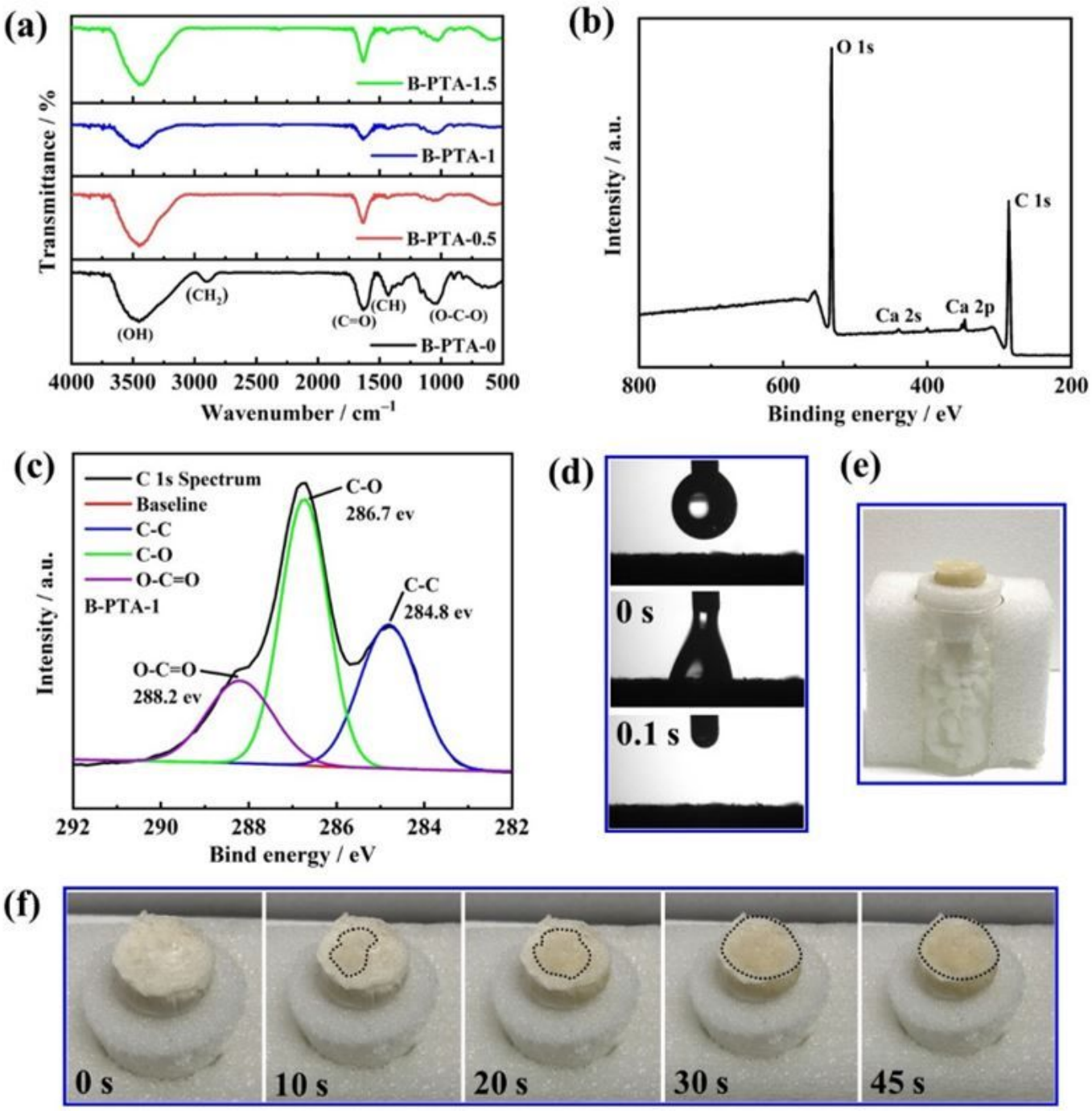

Figure 3

FT-IR spectra of B-PTA-0, B-PTA-0.5, B-PTA-1 and B-PTA-1.5 (a); XPS survey scan (b) and high-resolution C 1s spectra of B-PTA-1 (c); time-lapse snapshots of absorption of a water droplet by B-TPA-1 (d); the test setup for solar-steam generation (e); water transport ability of B-PTA-0, where black dashed line shows the border between wet and dry areas on B-PTA surface (f)

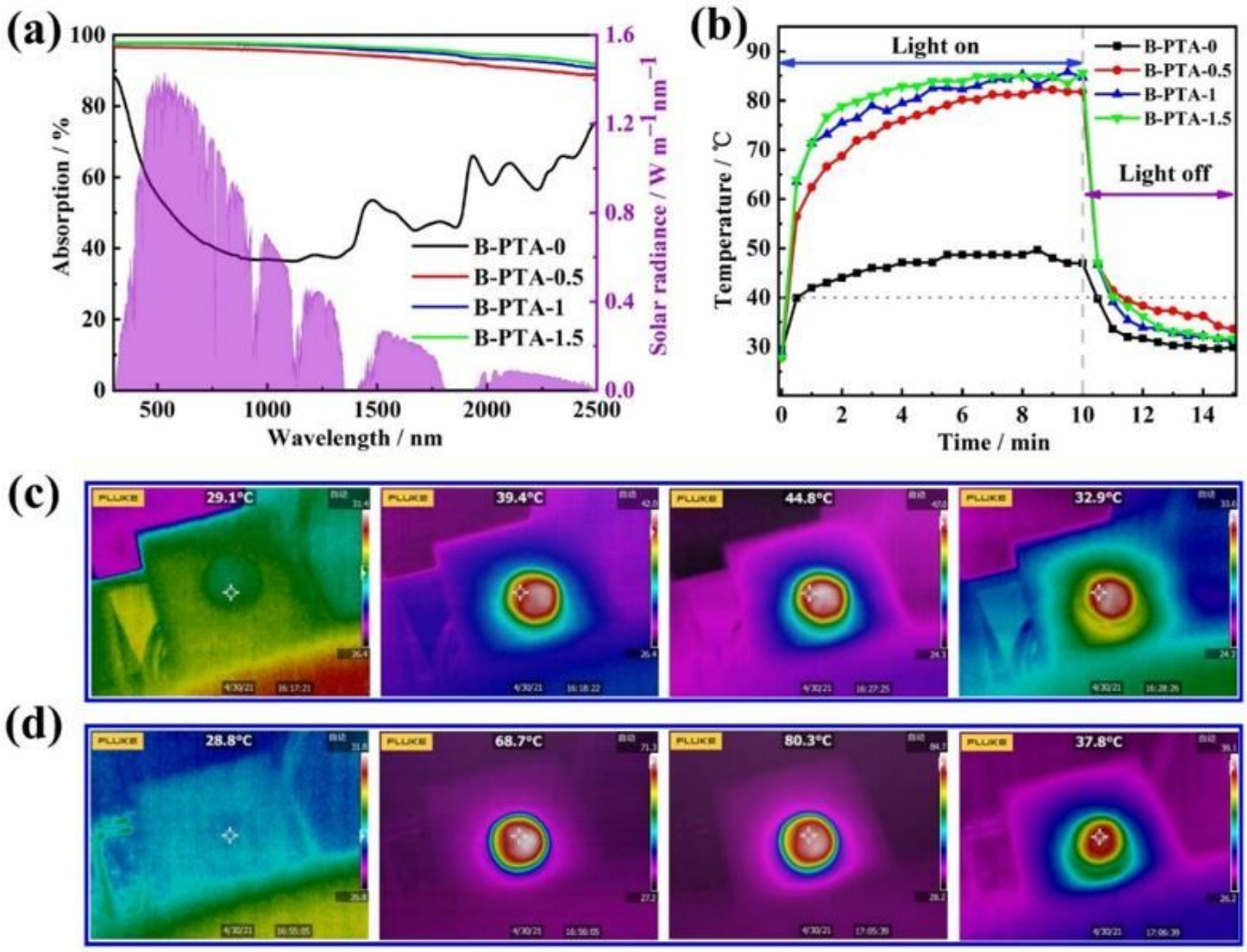

Figure 4

Absorption spectra of B-PTA-0, B-PTA-0.5, B-PTA-1 and B-PTA-1.5 together with solar spectral illumination (AM 1.5G, purple area) (a); time-dependent surface temperatures change of dry B-PTA-0, B-PTA-0.5, B-PTA-1 and B-PTA-1.5 under 1-sun irradiation in air (b); IR images of dry B-PTA-0 (c) and B-PTA-1 (d) under 1-sun illumination in the air for 0, 1, 10 minutes, and light off for 1 minute, respectively

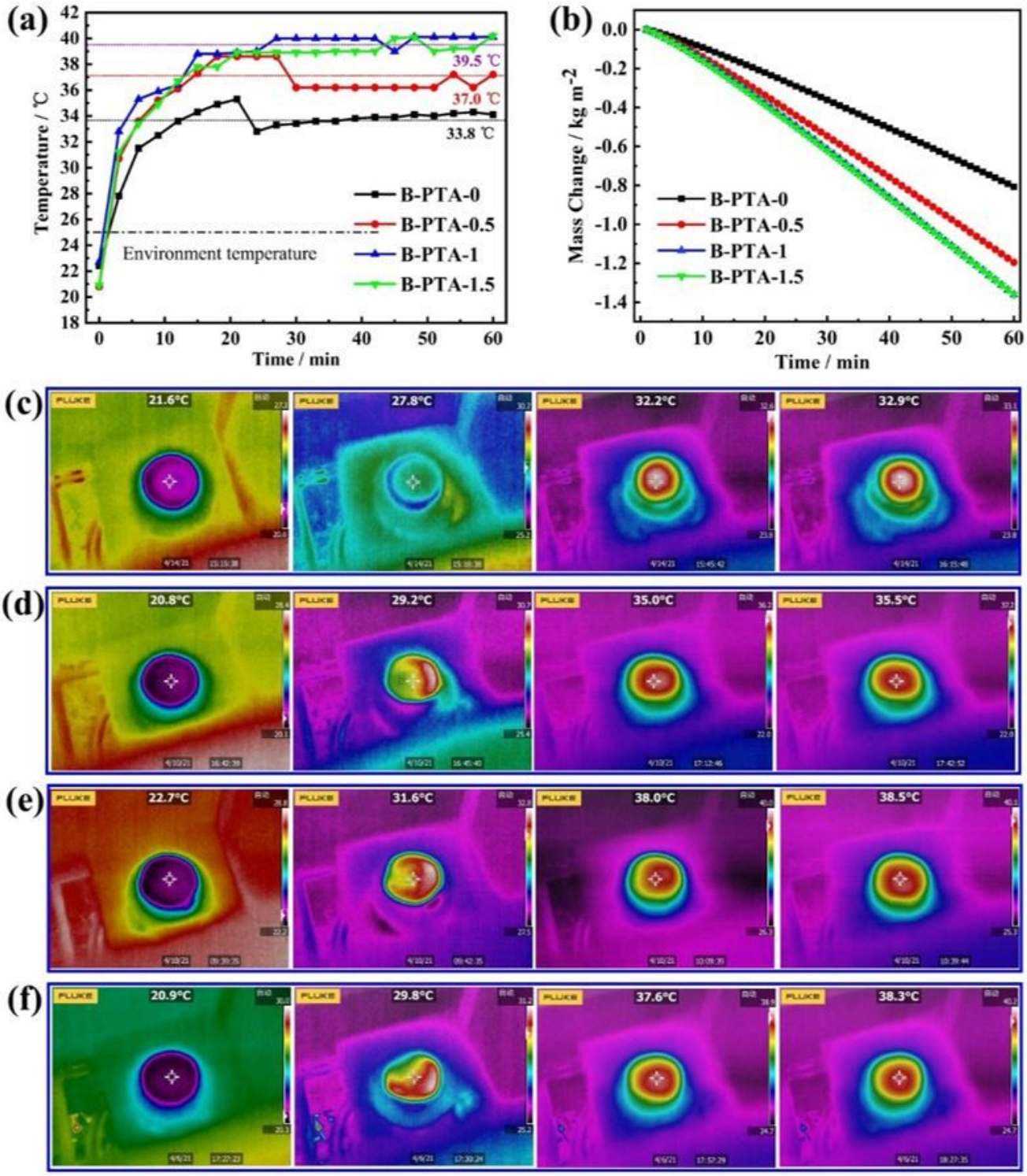

Figure 5

Time-dependent temperature of the top surface of wet B-PTA-0, B-PTA-0.5, B-PTA-1 and B-PTA-1.5 under 1-sun irradiation (a); Time-dependent weight loss of water of B-PTA-0, B-PTA-0.5, B-PTA-1 and B-PTA-1.5 (b); IR images of surface temperature of B-PTA-0 (c), B-PTA-0.5 (d), B-PTA-1 (e) and B-PTA-1.5 (f) at 0, 3, 30 and 60 minutes, respectively

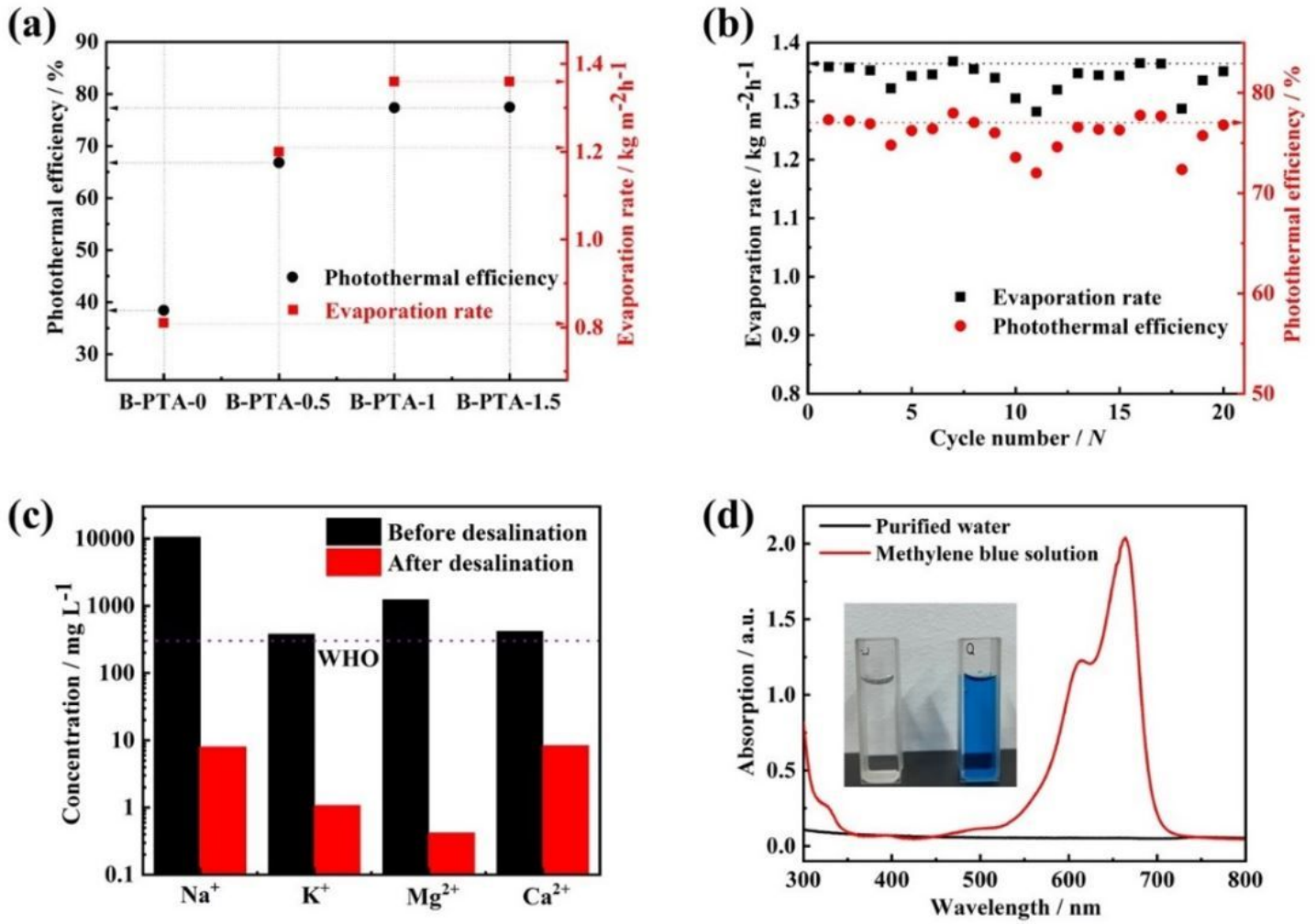

Figure 6

Photothermal efficiency of B-PTA-0, B-PTA-0.5, B-PTA-1 and B-PTA-1.5 (a); cycle evaporation performance of B-PTA-1 under 1-sun illumination (b); the measured concentrations of cations in a simulator seawater sample after solar thermal desalination (c); the UV–vis spectra of methyl blue solution (5 mg/L) before and after solar thermal purification (the inserts show the color of the solutions) (d)

Supplementary Files

This is a list of supplementary files associated with this preprint. Click to download.

- AuthortemplateforjournalarticlesLIMSI.docx